Iranian Journal of Astronomy and Astrophysics
Vol. 5, No. 1, Spring 2018

DOI:10.22128/ijaa.2018.144

Iranian Journal of Astronomy and Astrophysics

Magnetic field effects in the initial collapse of polytropic clouds

Seyed Bagher Ebrahimian Jelodar · Motahareh Mohammadpour*
School of Physics, Damghan University, Damghan, P.O.Box 36715-364, Iran;
email: mohammadpour@du.ac.ir

Abstract. In this paper, we investigate the influence of the magnetic field and the temperature gradients on the stability of a spherical cloud. Observational data confirm a power-law relation between the magnetic field and the gas density. Here, we study the stability of a magnetized cloud with a toroidal magnetic field and the polytropic equation of state. We find that density and mass profiles of the modified clouds are departed from the non-magnetized isothermal case. As the result, the critical mass, radius and density contrast at the onset of the gravitational instability differ from the critical Bonnor-Ebert mass and its critical radius and density contrast. Thus, both the magnetic field and the temperature gradients play important roles in the structure of the cloud. Furthermore, the cloud critical mass is increased for the higher values of the polytropic exponent, irrespective of the values of the magnetic to thermal pressure ratios or the field gradients. Different values of the magnetic field gradient and strength change the values of the critical density contrast and radius of the cloud; however, both of them fade their importance in the values of the critical mass.

Keywords: ISM: stars formation

1 Introduction

Stars are born in dense regions of molecular clouds when the pulling force of gravity overtakes the opposing forces. These dense regions mostly give birth to low-mass stars which compose a significant amount of the total visible mass in galaxies. The low-mass star-forming dense regions with temperatures of $7 - 20K$, comprise the mass of a few times the solar mass on scales of a few tenths of a parsec, have been extensively studied through theoretical modeling methods (e.g.,[1, 2, 3, 4]) and observational techniques (e.g.,[5, 6]), but much about these mysterious entities is still unknown.

Half of the observed dense cores have already contained embedded stars (e.g.,[7]), while the other ones are still starless (e.g.,[8]). It is now obvious that only a small fraction of the interstellar medium gas turns into stars [9]. This situation is absolutely inherited from an earlier stage, at the beginning of collapse process. Ebert (1955) [10] and Bonnor (1956) [11] investigated the stability of an isothermal spherical cloud in a hydrostatic equilibrium, called the Bonnor-Ebert sphere. A number of authors probed the stability of the modified Bonnor-Ebert sphere, from seeking the effect of chemistry [12], or the non-isothermal effects [13, 14], to finding the role of the ambient medium [15] on the core stability. Applying perturbation to the stable clouds is also used to prob the hydrodynamic evolution of a starless cloud for both the isothermal and non-isothermal clouds (e.g., [16, 17]), which showed that the cloud would finally start a slow, quasi-static, contraction, in consistent with observational studies [18]. In all the above-mentioned studies, the magnetic field effects were entirely ignored.

Magnetic fields have been revealed in the interstellar medium through a variety of observational techniques, e.g., Zeeman effects, polarized dust emission, or maser lines measurements, [19, 20, 21, 22]. Magnetic field plays an important role in the formation, stability and evolution of molecular clouds (e.g.,[24]). A number of authors use a power-law relation between the field strength and density (e.g.,[24]) which is parameterized as $B \propto \rho^n$, where n is a constant and the values of $n \lesssim 0.5$ are for the strong magnetic field [25], and $n \approx \frac{2}{3}$ is for the weak magnetic fields [26, 24].

Nejad-Asghar (2016) [27] investigated the effect of ambipolar diffusion heating, which is important in bringing the cloud to the point of gravitational instability, on the non-isothermal modified Bonnor-Ebert spheres and showed that the radius and mass of spheres are affected by the temperature gradients. Gholipour (2017) [28] studied the effect of magnetic field on the stability of a spherical isothermal cloud, and concluded that the magnetic field plays an important role in the structure of the cloud. He further extended this research and studied the stability of isothermal spherical and cylindrical clouds in the presence of the turbulent medium [29], and concluded that the shape of the clouds is important in the cloud structure.

Molecular clouds are subjected to the heating and cooling processes [30, 31] and the magnetic field of the interstellar medium [32]. Thus, to improve the understanding of the cloud stability, the magnetic field and the non-isothermal effects should be included. In the present paper, we study the effects of both the magnetic field and the temperature gradients on the cloud stability. For this purpose, we probe the temperature gradients, for simplicity, by a polytropic equation of state and use a power-law relation between the magnetic field and the gas density to investigate the initial cloud stability. Here, for simplicity, the cloud model is considered to be spherical; however, the real dense cores are most likely to have prolate shapes [33], and the rotational effects are ignored.

For the model of this paper, the gas magnetostatic equations and their nondimensionalization are introduced in section 2. Sections 3 gives numerical results. Finally, section 4 compares these results with other studies and gives conclusions.

2 Basic Equations

In this section, we consider a spherical cloud that maintains a magnetostatic equilibrium through the forces of Lorentz, self-gravity and thermal pressure. Thus, the force balance equation reads

$$-\nabla\phi = \frac{1}{\rho}\nabla P + \frac{1}{4\pi\rho}(\nabla \times B) \times B, \tag{1}$$

where B is the magnetic field, ϕ is the gravitational potential, ρ is the density and P is the gas pressure. The Poisson's equation relates the gravitational potential and the gas density as follows

$$\nabla^2\phi = 4\pi G\rho, \tag{2}$$

where G is the gravitational constant. The following integration over spherical shells of radius r gives the cloud mass, M, as follows

$$M = 4\pi \int_0^{r_0} \rho r^2 dr, \tag{3}$$

where r_0 is the cloud outer radius. In the spherical symmetry, the magnetic field can be described by poloidal, B_θ, and toroidal, B_ϕ, components. If the toroidal component is

dominant (i.e., $B_\theta \ll B_\phi$)(e.g.,[34]), then the magnetostatic equilibrium equation (eq. 1) becomes

$$\frac{d\phi}{dr} = -\frac{1}{\rho}\frac{dP}{dr} - \frac{1}{4\pi\rho}\frac{B_\phi}{r}\frac{d}{dr}\left(rB_\phi\right). \tag{4}$$

In spherical symmetry, the Poisson's equation becomes

$$\frac{1}{r^2}\frac{d}{dr}\left(r^2\frac{d\phi}{dr}\right) = 4\pi G\rho. \tag{5}$$

In this paper, the temperature gradient is regarded by a polytropic equation of state that relates the pressure and density as follows

$$P = K\,\rho^{1+\frac{1}{n'}} \;=\; K\,\rho^{\gamma}, \tag{6}$$

where K is a constant and n' is the polytopic index. For simplicity, we set $\gamma = 1 + \frac{1}{n'}$, where γ is the polytropic exponent. We use a power-law relation between the magnetic field strength and the gas density as follows

$$B = \alpha\rho^n, \tag{7}$$

where n, the power-law exponent which indicates the field gradient, and α, the field strength, are constants. We substitute the relations (6) and (7) into the equation (4), and find the following relation

$$\frac{d\phi}{dr} = -\left[K\gamma\rho^{\gamma-2}\,\frac{d\rho}{dr} + \frac{\alpha^2\rho^{2n-1}}{4\pi r}\left(1 + \frac{nr}{\rho}\frac{d\rho}{dr}\right)\right]. \tag{8}$$

We notice that the gravitational force per unit mass, $d\phi/dr$, is $-GM(r)/r^2$, where $M(r)$, the mass within any radius approaches $4\pi\rho_c r^3/3$ in spherical coordinates in that ρ_c is the central density. Then, $d\phi/dr$ disappears as r goes to zero. From the equation (8), we find that

$$\lim_{r\to 0}\frac{d\rho}{dr} = \frac{-\alpha^2\rho^{2n-\gamma+1}}{4\pi K r}\left(\gamma + \frac{n\alpha^2\rho^{2n-\gamma}}{4\pi K}\right)^{-1}, \tag{9}$$

which shows that although $\frac{d\rho}{dr}(r=0)$ is zero for the non-magnetic cases, it is no longer zero with the inclusion of the magnetic field effects. We substitute the equation (8) into the Poisson's equation (5), which reads

$$\frac{d}{dr}\left[r^2K\gamma\rho^{\gamma-2}\frac{d\rho}{dr} + \frac{r\alpha^2\rho^{2n-1}}{4\pi}\left(1 + \frac{nr}{\rho}\frac{d\rho}{dr}\right)\right] = -4\pi G\rho r^2. \tag{10}$$

The density is given by

$$\rho = \rho_c\varrho, \tag{11}$$

where ρ_c is the central density and ϱ is the non-dimensional density. We substitute the relation (11) into the equation (10), which reads

$$\frac{d}{dr}\left(r^2\gamma K\rho_c^{\gamma}\varrho^{(\gamma-2)}\frac{d\varrho}{dr} + \frac{r\alpha^2\rho_c^{2n}}{4\pi}\varrho^{(2n-1)} + \frac{nr^2\alpha^2\rho_c^{2n}}{4\pi}\varrho^{(2n-2)}\frac{d\varrho}{dr}\right) = -4\pi G\rho_c^2 r^2\varrho. \tag{12}$$

By defining $P_c = K\rho_c^{\gamma}$ and $B_c^2 = \alpha^2\rho_c^{2n}$, where P_c is the central pressure and B_c is the central magnetic field, the equation (12) develops into

$$\frac{d}{dr}\left(r^2\gamma\varrho^{(\gamma-2)}\frac{d\varrho}{dr} + \frac{rB_c^2}{4\pi P_c}\varrho^{(2n-1)} + \frac{nr^2B_c^2}{4\pi P_c}\varrho^{(2n-2)}\frac{d\varrho}{dr}\right) = -\frac{4\pi G\rho_c^2 r^2}{P_c}\varrho. \tag{13}$$

Here, we introduce the dimensionless length ξ as

$$\xi = (\frac{4\pi G\rho_c^2}{P_c})^{\frac{1}{2}}\ r, \tag{14}$$

to recast equation (13) into non-dimensional form as follows

$$\frac{d}{d\xi}\left(\gamma\,\xi^2\,\varrho^{(\gamma-2)}\,\frac{d\varrho}{d\xi} + 2\,\lambda\,\xi\,\varrho^{(2n-1)} + 2\,n\,\lambda\,\xi^2\,\varrho^{(2n-2)}\,\frac{d\varrho}{d\xi}\right) = -\xi^2\,\varrho, \tag{15}$$

where the parameter

$$\lambda = \frac{B_c^2}{8\pi P_c}, \tag{16}$$

is the ratio of magnetic to thermal pressure in the center of cloud. From the equation (15), we have

$$\begin{aligned}
&\left(\gamma\varrho^{(\gamma-3)} + 2\lambda n\varrho^{(2n-3)}\right)\frac{d^2\varrho}{d\xi^2} \\
&+ \left(2\gamma\varrho^{(\gamma-3)} + 2\lambda(4n-1)\varrho^{(2n-3)}\right)\frac{1}{\xi}\left(\frac{d\varrho}{d\xi}\right) \\
&+ \left(\gamma(\gamma-2)\varrho^{(\gamma-4)} + 4\lambda n(n-1)\varrho^{(2n-4)}\right)\left(\frac{d\varrho}{d\xi}\right)^2 \\
&+ \frac{2\lambda}{\xi^2}\varrho^{(2n-2)} + 1 = 0,
\end{aligned} \tag{17}$$

The inner boundary condition are $\varrho(\xi=0)=1$ and $\frac{d\varrho}{d\xi}(\xi=0)$ is given from (9) as follows

$$\lim_{\xi\to 0}\frac{d\varrho}{d\xi} = -\frac{2\lambda}{\xi}\varrho^{(2n-\gamma+1)}\left(\gamma + 2\lambda n\varrho^{(2n-\gamma)}\right)^{-1}, \tag{18}$$

from which $\frac{d\varrho}{d\xi}(\xi=0)=0$ is derived for the non-magnetic cases, i.e, $\lambda=0$. The solutions of the equation (17) with the mentioned inner boundary conditions give the density at any radius. Now, if the cloud is surrounded by an isothermal medium with the dimensional pressure, sound speed and density denoted by P_0, a_T and ρ_0, and the dimensional cloud outer radius is denoted by r_0, the dimensional mass is calculated as

$$m = 4\pi\int_0^{r_0} r^2\rho(r)dr = \frac{4\pi\rho_c}{\left(\frac{4\pi G\rho_c^2}{P_c}\right)^{\frac{3}{2}}}\int_0^{\xi_0}\xi^2\varrho d\xi. \tag{19}$$

From the equations (15) and (19), we have

$$m = \frac{P_c^{\frac{3}{2}}}{(4\pi)^{\frac{1}{2}}\,G^{\frac{3}{2}}\rho_c^2}\left(\gamma\,\xi^2\,\varrho^{(\gamma-2)}\,\frac{d\varrho}{d\xi} + 2\,\lambda\,\xi\,\varrho^{(2n-1)} + 2\,n\,\lambda\,\xi^2\,\varrho^{(2n-2)}\,\frac{d\varrho}{d\xi}\right)_{\xi_0}. \tag{20}$$

Now, we define the non-dimensional mass, M, as follows

$$\begin{aligned}
M &\equiv \frac{(4\pi p_0)^{\frac{1}{2}}G^{\frac{3}{2}}m}{a_T^4} \\
&= \left(\frac{\rho_c}{\rho_0}\right)^{\frac{3}{2}\gamma-2}\left(\gamma\xi^2\,\varrho^{(\gamma-2)}\frac{d\varrho}{d\xi} + 2\lambda\xi^2\varrho^{(2n-1)}\left(\frac{n}{\varrho}\frac{d\varrho}{d\xi} + \frac{1}{\xi}\right)\right)_{\xi_0}.
\end{aligned} \tag{21}$$

We solve the equations (17) and (21) numerically with the mentioned inner boundary conditions to obtain the non-dimensional density and mass in next section.

3 Results

In this section, we use the Runge-Kutta-Fehlberg method and the bifurcation technique [35] to solve the differential equations (17) and (21) with the mentioned inner boundary conditions, $\varrho(0) = 1$ and (18). Fig.1, left panel, displays the nondimensional density, $\varrho = \rho/\rho_c$, as a function of the cloud nondimensional radius, ξ, for different values of the magnetic to thermal pressure ratios, λ, and a same value of the field power-law exponent of $n = \frac{2}{3}$. The density profiles of $\gamma = 0.8$, $\gamma = 1.0$ and $\gamma = 1.2$, for different values of $\lambda = 0, \frac{1}{16}, \frac{1}{8}, \frac{1}{4}$ and 1, are shown in Fig.1(a), Fig.1(c) and Fig.1(e), respectively. The figures show that the densities, and hence both the thermal and magnetic pressures, fall away gradually from the center of the cloud for all the three selected values of γ, as a result of the magnetostatic configurations. The gradual drop, for the value of each γ becomes steeper for the higher values of λ, which shows that the magnetic field strength plays an important role in the configuration. Besides, as the profiles show, the drop, for the each value of λ, is stronger for the higher values of γ, as a result of the higher gas thermal pressures which support the cloud against gravity. For small radii, $log(\xi) < 0$, the slope of the density profiles for each γ is approximately zero for $\lambda = 0$ and increases with higher values of λ, that can be inferred from the equation (18) of the present paper and is consistent with the work of Gholipour (2017) [28].

Since the density is ρ_c at the center of the cloud and ρ_0 at the edge of the cloud, ρ/ρ_c is 1.0 at the beginning of all plots and drops to a minimum value at its edge. Thus, a certain density contrast, ρ_c/ρ_0, implies a certain nondimensional radius which can be found from the Fig.1 for each case. The case with $\lambda = 0$ and $\gamma = 1$ is the characterization of an isothermal gas in a hydrostatic equilibrium. As it is obvious from Fig.1, the consideration of different values of λ and γ departs the profiles from the isothermal case, which is itself in the hydrostatic equilibrium.

Fig.1, right panel, displays the nondimensional mass, M, of a pressure-bounded cloud as a function of the logarithm of density contrast from the center to the edge, $log(\rho_c/\rho_0)$, for different values of λ, and a same value of $n = \frac{2}{3}$. The mass profiles of $\gamma = 0.8$, $\gamma = 1.0$ and $\gamma = 1.2$, for different values of $\lambda = 0, \frac{1}{16}, \frac{1}{8}, \frac{1}{4}$ and 1, are shown in Fig.1(b), Fig.1(d) and Fig.1(f), respectively. $\xi = 0$ implies $M = 0$ at the beginning of all plots. In all plots, M first rise to a maximum critical value, M_{cr}, where we can find the corresponding critical density contrast, $(\frac{\rho_c}{\rho_0})_{cr}$. Then, the mass turns over for the greater density contrasts. The turnover marks the onset of gravitational instability, i.e., those clouds with $(\frac{\rho_c}{\rho_0}) > (\frac{\rho_c}{\rho_0})_{cr}$ are gravitationally unstable. The lower density contrasts, i.e., those clouds with $(\frac{\rho_c}{\rho_0}) < (\frac{\rho_c}{\rho_0})_{cr}$, are confined by the external pressure and are gravitationally stable. To see why any increase of P_0 at fixed a_T and the cloud dimensional mass, m, causes the cloud nondimensional mass, M, to rise from the equation (21), and hence $(\frac{\rho_c}{\rho_0})$ to rise for clouds of low density contrast from Fig.1, which creates a rise in the internal pressures. As the result, the cloud remains stable. The critical mass for $\lambda = 0$ and $\gamma = 1$ is the well-known Bonnor-Ebert mass.

For any critical density contrast, the corresponding critical radius, ξ_{cr}, can be found from the corresponding density profiles in Fig.1. The critical values of radius, density contrast and mass of $n = \frac{2}{3}$, for different values of λ and γ, are presented in Table.1. This table shows that the cloud with the higher values of γ has more critical mass for the value of each λ, since higher thermal pressures can help stave off collapse. Thus, the cloud with $\gamma = 1.2$ shows the higher $(\frac{\rho_c}{\rho_0})_{cr}$ and M_{cr} than $\gamma = 1.0$ and 0.8 for any values of λ.

While the critical density contrast and radius, for each γ, increase for the higher values of λ, there are some slight changes in the critical mass of the corresponding cases. The critical mass of $n = \frac{2}{3}$ as a function of λ, for $\gamma = 0.8$, $\gamma = 1.0$ and $\gamma = 1.2$, is plotted in Fig.3(a).

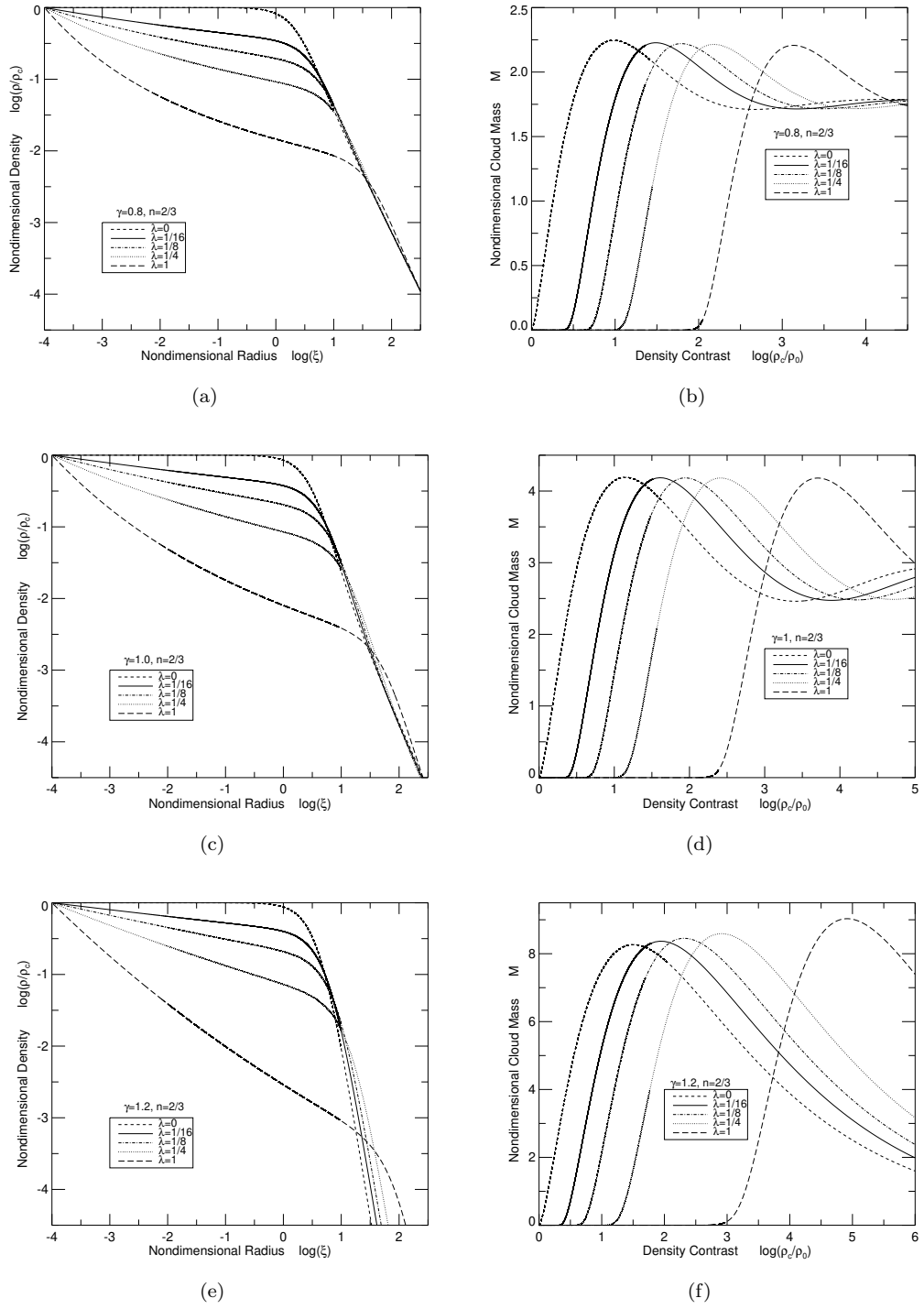

Figure 1: Left panel: Nondimensional density profiles, ρ/ρ_c, of $n = 2/3$ and different magnetic to thermal pressure ratios, λ, as a function of the cloud nondimensional radius, ξ, for $\gamma = 0.8$, $\gamma = 1.0$ and $\gamma = 1.2$. Right panel: Nondimensional mass profiles, M, of $n = 2/3$ and different magnetic to thermal pressure ratios, λ, as a function of density contrast, ρ_c/ρ_0, for $\gamma = 0.8$, $\gamma = 1.0$ and $\gamma = 1.2$.

Table 1: Results of the calculations for $n = \frac{2}{3}$. From left to right, the columns are: states for the three different values of the polytropic exponents with different values of the magnetic to thermal pressure ratios; critical value of radius; critical value of density contrast; critical value of mass.

$n = \frac{2}{3}$, $\gamma = 0.8$	ξ_{cr}	$(\frac{\rho_c}{\rho_0})_{cr}$	M_{cr}
$\lambda = 0$	5.8	9.7	2.3
$\lambda = \frac{1}{16}$	11.9	32.0	2.2
$\lambda = \frac{1}{8}$	17.9	63.3	2.2
$\lambda = \frac{1}{4}$	30.4	152.8	2.2
$\lambda = 1$	116.4	1.43×10^3	2.2
$n = \frac{2}{3}$, $\gamma = 1.0$	ξ_{cr}	$(\frac{\rho_c}{\rho_0})_{cr}$	M_{cr}
$\lambda = 0$	6.5	14.1	4.2
$\lambda = \frac{1}{16}$	10.9	40.2	4.2
$\lambda = \frac{1}{8}$	15.9	85.6	4.2
$\lambda = \frac{1}{4}$	27.9	266.0	4.2
$\lambda = 1$	126.4	5.5×10^3	4.2
$n = \frac{2}{3}$, $\gamma = 1.2$	ξ_{cr}	$(\frac{\rho_c}{\rho_0})_{cr}$	M_{cr}
$\lambda = 0$	7.4	32.1	8.3
$\lambda = \frac{1}{16}$	10.9	84.5	8.4
$\lambda = \frac{1}{8}$	15.4	201.3	8.5
$\lambda = \frac{1}{4}$	27.4	859.0	8.6
$\lambda = 1$	181.4	9.44×10^4	9.0

This Figure shows that M_{cr} is slightly affected by the field strength for the selected values of λ.

Fig.2, left panel, displays the nondimensional density, ρ/ρ_c, as a function of the cloud nondimensional radius, ξ, for a same value of the magnetic to thermal pressure ratio of $\lambda = \frac{1}{10}$, and different values of the polytropic exponents. The density profiles of the field power-law exponent of $n = \frac{2}{3}$, $n = \frac{5}{9}$ and $n = \frac{4}{9}$, for different values of $\gamma = 0.8, 0.9, 1.0, 1.1$ and 1.2, are shown in Fig.2(a), Fig.2(c) and Fig.2(e), respectively. The figures show that the densities, for all values of γ, fall away from the center of the cloud for all the three selected values of n, as a result of the magnetostatic configuration. The gradual drop, for each γ, becomes steeper for the lower values of n, which shows that the magnetic field gradient plays an important role in the configuration. Besides, as the profiles show, the drop, for each n, is stronger for the higher values of γ, in large radii of the cloud.

Fig.2, right panel, displays the nondimensional mass, M, of a pressure-bounded cloud as a function of the logarithm of density contrast from the center to the edge, $log(\rho_c/\rho_0)$, for different values of γ, and a same value of $\lambda = \frac{1}{10}$. The mass profiles of $n = \frac{2}{3}$, $n = \frac{5}{9}$ and $n = \frac{4}{9}$, for different values of $\gamma = 0.8, 0.9, 1.0, 1.1$ and 1.2, are shown in Fig.2(b), Fig.2(d) and Fig.2(f), respectively. In all plots, M first rises to a maximum critical value, M_{cr}, then it turns over for the greater density contrasts. For the lower values of n, i.e., $n \lesssim 0.5$ which characterize the strong magnetic field, the turnovers occur at higher density contrasts, and hence higher critical radii, for each value of γ. The critical values of radius, density contrast and mass of $\lambda = \frac{1}{10}$, for different values of n and γ, are presented in Table.2.

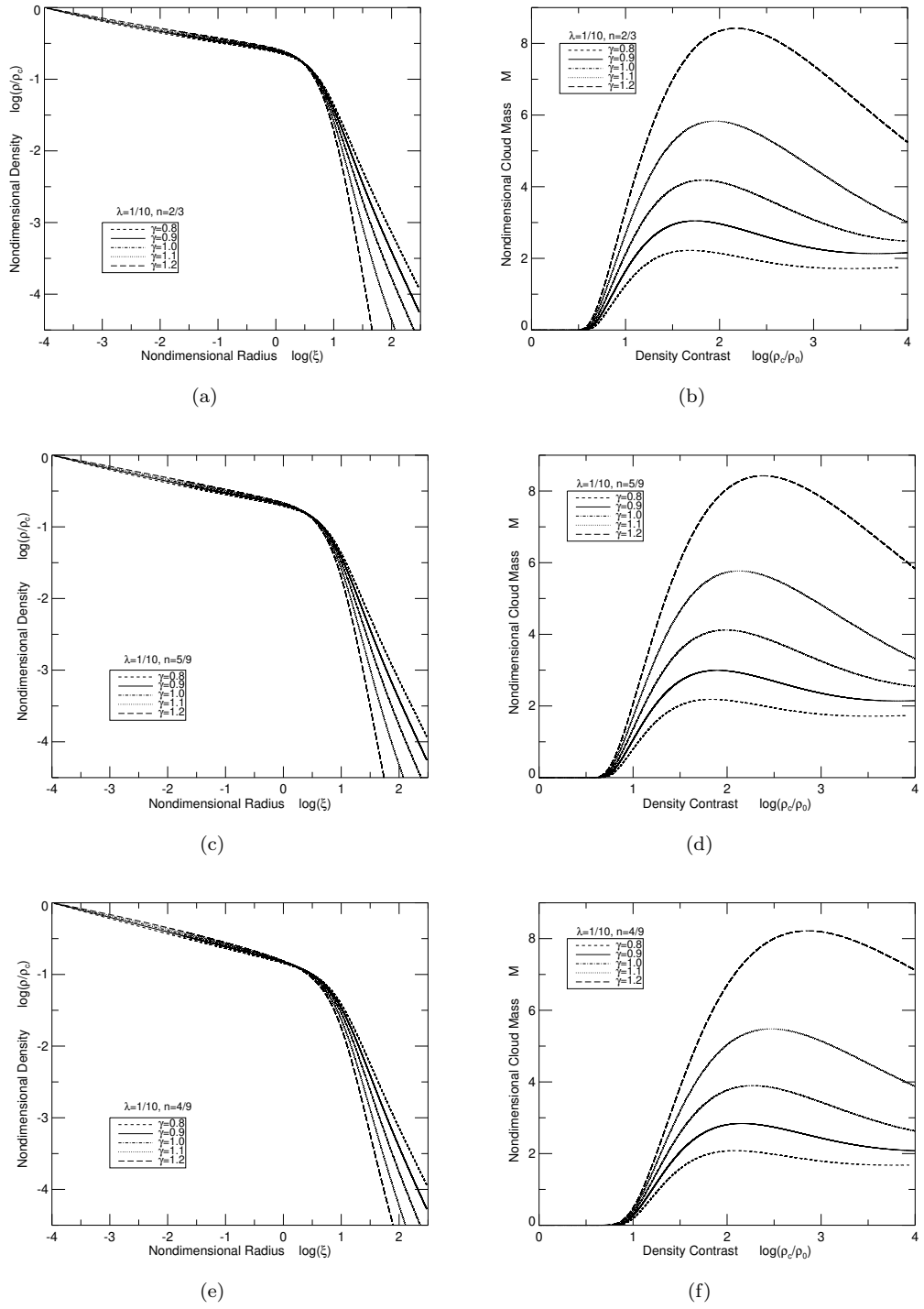

Figure 2: Left panel: Nondimensional density profiles, ρ/ρ_c, of $\lambda = 1/10$ and different polytropic exponents, γ, as a function of the cloud nondimensional radius, ξ, for $n = 4/9$, $n = 5/9$ and $n = 2/3$. Right panel: Nondimensional mass profiles, M, of $\lambda = 1/10$ and different polytropic exponents, λ, as a function of density contrast, ρ_c/ρ_0, for $n = 4/9$, $n = 5/9$ and $n = 2/3$.

Table 2: Results of the calculations for $\lambda = \frac{1}{10}$. From left to right, the columns are: states for the three different values of the magnetic field power-law exponents for different values of the polytropic exponents; critical value of radius; critical value of density contrast; critical value of mass.

$n = \frac{2}{3}$, $\lambda = \frac{1}{10}$	ξ_{cr}	$(\frac{\rho_c}{\rho_0})_{cr}$	M_{cr}
$\gamma = 0.8$	14.3	43.6	2.2
$\gamma = 0.9$	13.7	49.2	3.0
$\gamma = 1.0$	13.2	59.0	4.2
$\gamma = 1.1$	12.9	79.0	5.8
$\gamma = 1.2$	12.9	131.2	8.4
$n = \frac{5}{9}$, $\lambda = \frac{1}{10}$	ξ_{cr}	$(\frac{\rho_c}{\rho_0})_{cr}$	M_{cr}
$\gamma = 0.8$	17.2	59.7	2.2
$\gamma = 0.9$	16.2	67.9	3.0
$\gamma = 1.0$	15.4	82.5	4.1
$\gamma = 1.1$	15.0	112.8	5.8
$\gamma = 1.2$	15.2	200.0	8.4
$n = \frac{4}{9}$, $\lambda = \frac{1}{10}$	ξ_{cr}	$(\frac{\rho_c}{\rho_0})_{cr}$	M_{cr}
$\gamma = 0.8$	22.9	99.7	2.1
$\gamma = 0.9$	21.2	114.8	2.8
$\gamma = 1.0$	20.0	145.1	3.9
$\gamma = 1.1$	19.6	216.0	5.5
$\gamma = 1.2$	21.0	488.3	8.2

While the values of the critical density contrast and radius, for each γ, change for the different values of n, there are some slight changes in the corresponding critical mass. The values of the critical mass of $\lambda = \frac{1}{10}$ as a function of n, for $\gamma = 0.8$, $\gamma = 1.0$ and $\gamma = 1.2$, are plotted in Fig.3(b). This figure shows that M_{cr} is slightly affected by the field gradient for the selected values of n.

4 Discussion

In this paper, we have studied the effects of temperature gradients on the stability of a magnetized cloud with a toroidal magnetic field configuration. The cloud model in the magnetostatic configuration has been considered to have a spherical shape. The temperature gradients has been included in the model by a polytropic equation of state, and the magnetic field has been expressed by a power-law relation with the gas density, irrespective to the origin of the magnetic field.

We probed how the inclusion of both the temperature gradients and the magnetic field effects depart the stability criteria of a spherical cloud, i.e., the critical density contrast, the critical radius and the mass, from the isothermal one in the hydrostatic equilibrium.

The results of the present paper showed that the density and mass profiles of the modified cloud, with the inclusion of the temperature gradients and the magnetic field effects, are departed from the non-magnetized isothermal case, is consistent with the previous studies [27, 28]. Furthermore, only a limited subset of the model is shown to be gravitationally

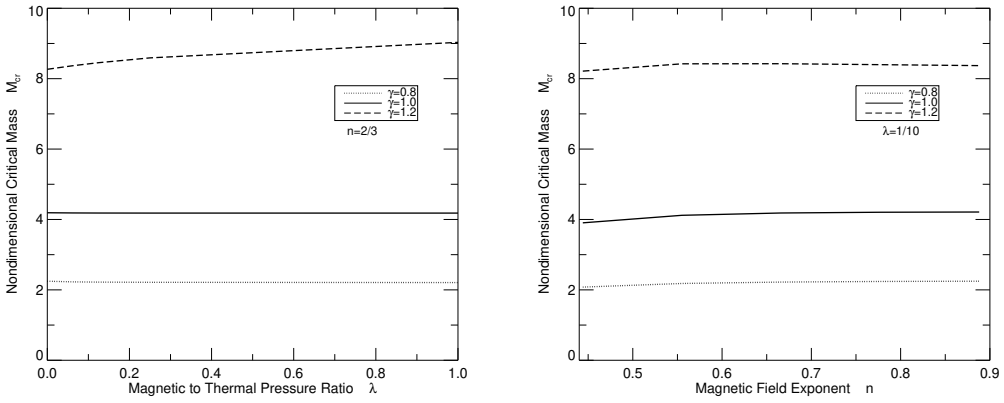

(a) (b)

Figure 3: Left panel: Profile of critical mass as a function of λ, for $n = \frac{2}{3}$. Right panel: Profile of critical mass as a function of n, for $\lambda = \frac{1}{10}$. The lines represent $\gamma = 0.8$, $\gamma = 1.0$ and $\gamma = 1.2$

stable. The critical mass, radius and density contrast of the the gravitationally stable clouds, i.e., the maximum mass allowed by the polytropic sphere to hold the magnetostatic configuration and its corresponding critical density contrast and radius, are departed from the Bonnor-Ebert mass for different values of the polytropic exponents, the magnetic field gradients and strengths. The results showed that the critical mass is increased for the higher values of the polytropic exponents, irrespective of the magnetic to thermal pressure ratios or the field gradients.

The results of the present paper showed that the magnetic field plays an important role in the structure of the cloud. However, different values of the magnetic field gradient and strength change the critical density and radius of the model, both of them fade their importance in the values of the critical mass for each polytropic exponent.

However, magnetic field is likely responsible for reducing the star formation rate in dense cores [36], it may not play any role in the total mass of the cloud [37]. Besides, dense core may have transient, out-of-equilibrium structures [38], instead of having quasi-magnetostatic configurations. For a better understanding of the stability criteria, an account for the heating and cooling processes and the rotational effects should be included.

Acknowledgements

The authors would like to thank the referee for useful comments.

References

[1] Alves, J. F., Lada, C. J., & Lada, E. A. 2001, Nature, 409, 159

[2] Larson, R. B. 1969, MNRAS, 145, 271

[3] Shu, F. H. 1977, ApJ, 214, 488

[4] Foster, P. N., & Chevalier, R. A. 1993, ApJ, 416, 30

[5] Lee, C. W., Myers, P. C., & Tafalla, M. 2001, ApJS 136, 703

[6] Goodman, A. A., Barranco, J. A., Wilner, D. J., & Heyer, M. H. 1998, ApJ, 504,22

[7] Jessop, N. E., & Ward-Thompson, D. 2000, MNRAS, 311, 63

[8] Tafalla, M., Myers, P. C., Caselli, P., & Walmsley, C. M. 2004, A&A, 416,181

[9] Elmegreen, B. G. 2000, ApJ, 530, 277

[10] Ebert, R. 1955, Z. Astrophys., 37, 217

[11] Bonnor, W. B. 1956, MNRAS, 116, 351

[12] Sipilä, O., Caselli, P., & Juvela, M. 2017, A&A, 601, 113

[13] Sipilä, O., Harju, J., & Juvela, M. 2015, A&A, 582, 48

[14] Sipilä, O., Harju, J., & Juvela, M. 2011, A&A, 535, 49

[15] Kaminski, E., Frank, A., Carroll, J., & Myers, P. 2014, ApJ, 790, 70

[16] Stahler, S. W., & Yen, J. J. 2009, MNRAS, 396, 579

[17] Khesali, A., Nejad-Asghar, M., & Mohammadpour, M. 2013, MNRAS, 430, 961

[18] Lee, C. W., & Myers, P. C. 2011, ApJ, 734, 60

[19] Crutcher, R. M. 1999, ApJ, 520, 706

[20] Troland, T. H., & Crutcher, R. M. 2008, ApJ, 680, 457

[21] Mouschovias, T. Ch., & Tassis, K. 2009, MNRAS, 400, 15

[22] Mouschovias, T. Ch., & Tassis, K. 2010, MNRAS, 409, 801

[23] Tritsis, A., Panopoulou, G. V., Mouschovias, T. C., Tassis, K., & Pavlidou, V. 2015, MNRAS, 451, 4384

[24] Crutcher, R. M. 2012, ARA&A, 50, 29

[25] Mouschovias, T.C., & Ciolek, G. E. 1999, The Origin of Stars and Planetary Systems, ed. C. J. Lada & N. D. Kylafis (Dordrecht: Kluwer), 305

[26] Mestel, L. 1966, MNRAS, 133, 265

[27] Nejad-Asghar, M. 2016, Ap&SS, 361, 384

[28] Gholipour, M. 2017, ApJ, 838, 140

[29] Gholipour, M. 2018, New Astron., 69, 77

[30] Goldsmith, P. F., & Langer, W. D. 1978, ApJ, 222, 881

[31] Goldsmith, P. F. 2001, ApJ, 557, 736

[32] Clark, S. E. 2017, Ph.D. thesis, Columbia University

[33] Ryden, B. S. 1996, ApJ, 471, 822

[34] Novak, G., Chuss, D. T., Renbarger, T., Griffin, G. S., & et.al. 2003, ApJ, 583, L83

[35] Dalba, P. A., & Stahler, S. W. 2012, MNRAS, 425, 1591

[36] Hennebelle, P., & Inutsuka, S. 2019, FrASS, 6, 5H

[37] Shu, F. H., Adams, F. C., & Lizano, S. 1987, ARA&A, 25, 23

[38] Vazguez-Semadini, E. H., Kim, J., Shadmehri, M., & Ballesteros-Paredes, J. 2005, ApJ, 618, 344